J. Plasma Physics (2007), *vol.* 73, *part* 2, *pp.* 199–206. © 2006 Cambridge University Press
doi:10.1017/S0022377806004466 First published online 4 May 2006 Printed in the United Kingdom

Comparison between fluid electron-temperature-gradient driven simulations and Tore Supra experiments on electron heat transport

B. LABIT[1] and M. OTTAVIANI[2]

[1]École Polytechnique Fédérale de Lausanne,
Centre de Recherches en Physique des Plasmas,
Association Euratom-Confédération helvétique,
CH-1015 Lausanne

[2]Association EURATOM-CEA sur la Fusion,
CEA/DSM/DRFC, CEA Cadarache,
13108 Saint Paul lez Durance, France

(Received 7 February 2006)

Abstract. In recent years, much attention has been devoted to the electron-temperature-gradient (ETG) driven instability as a possible explanation for the high electron thermal conductivity found in most tokamaks. The present contribution assesses whether a specific three-dimensional fluid ETG model can reproduce the conductivity observed in the Tore Supra tokamak [Equipe Tore Supra (presented by R. Aymar) 1989 *Plasma Physics and Controlled Nuclear Fusion Research* (*Proc. 12th Int. Conf., Nice, 1988, Vol. 1.*) Vienna: IAEA, p. 9]. Although the model reproduces fairly well the observed critical gradient, a large discrepancy factor, of the order of 50, is found for the ratio between the experimental and the simulated conductivity. On the basis of this study, one must conclude that the electron heat transport cannot be explained only with a fluid ETG turbulence model.

1. Introduction

Heat transport in a tokamak is caused by plasma microturbulence driven by the equilibrium profiles. This turbulence strongly enhances the heat conductivities in both the ion and the electron channels. For many years, theoretical effort focused on ion heat losses, and particularly on the ion-temperature-gradient (ITG) driven turbulence characterized by perpendicular wavelengths in the ion gyroradius range [1]. The turbulence associated with this instability is now considered as the most likely explanation of the observed ion conductivity. Moreover, some authors have combined the trapped electron modes (TEM) with the ITG instability in order to explain the heat losses observed on the electron channel. Although they give the right order of magnitude, collisional TEM and collisionless TEM do not reproduce the dependence of the electron thermal conductivity observed in Tore Supra [2], $\chi_e \propto T_e^{1/2}/n_e$, where T_e is the electron temperature and n_e is the plasma density. On the other hand, it is interesting to note that this dependence is in agreement with Ohkawa's heuristic formula [3] $\chi_e \sim (cv_{th,e}/qR\omega_{pe})^2$, where ω_{pe} is the electron plasma frequency, $v_{th,e}$ the thermal velocity, q the safety factor and R

https://doi.org/10.1017/S0022377806004466 Published online by Cambridge University Press

the major radius. When written in dimensionless units, Ohkawa's formula makes explicit its dependence on the plasma β, since then $\chi_e/\chi_B \sim \rho_\star/\beta$, where χ_B is the Bohm conductivity and $\rho_\star$ is the normalized gyroradius. One has to note that, experimentally, it is very difficult to extract a scaling law for χ_e versus β keeping all the other dimensionless parameters constant [4].

So theorists and modellers have started considering the sub-ρ_i scale electron-temperature-gradient (ETG) modes that are driven by the temperature gradient of passing electrons as a possible cause of the observed electron heat transport. At the end of the 1980s, previous work [5–7] emphasized the intrinsic electromagnetic nature of this instability. The plasma skin depth δ_e comes in as a typical scale length, and one particular version of the mixing length estimate for χ_{ETG} is compatible with the Ohkawa's heuristic formula.

In the recent years, gyrokinetic simulations [8–10] have revisited the ETG instability. These authors have remarked that an exact isomorphism between ITG and ETG turbulence would give a turbulent electron heat transport $\chi_e/\chi_i \sim (m_e/m_i)^{1/2}$ too small, when compared with the experimental observations. Nevertheless, they reported that observed electron heat transport from flux tube gyrokinetic simulations is sufficiently large after all. The explanation given by Jenko et al. [8] is the generation of radially extended structures, called streamers, which occur because zonal flows are less effective as a consequence of the different adiabatic density response proper to the ETG and to the ITG models. They also reported that the $\mathbf{E} \times \mathbf{B}$ advection term dominates over the magnetic flutter term. Moreover, very recent global gyrokinetic simulations [11, 12] have confirmed that streamers are the typical nonlinear structures of the ETG turbulence, but in [12] this fact does not lead to the high turbulent transport as observed in experimental estimations and flux-tube simulations.

Finally, the electron heat transport caused by ETG turbulence was studied with a three-dimensional fluid electromagnetic code [13] by Labit and Ottaviani. In [14], the formation of streamers as observed in gyrokinetic simulations was reported. We also found that the electrostatic $\mathbf{E} \times \mathbf{B}$ transport term is much greater than that associated with magnetic flutter. Moreover, a gyro-Bohm dependence of electron transport was reported ($\chi_e \propto \rho_\star$) with a weak dependence on β. The lack of strong dependence on β is in contradiction with Ohkawa's formula, while a turbulent conductivity proportional to $\rho_\star$ is in agreement with this heuristic formula and also with experimental transport studies. Finally, our fluid simulations give an electron turbulent transport much lower when compared with gyrokinetic simulations, the presence of streamers notwithstanding.

The goal of this article is to assess whether ETG fluid electromagnetic simulations can reproduce the electron heat losses measured in the tokamak Tore Supra [15]. This paper is organized as follows. In Sec. 2, the main features of our global electromagnetic fluid ETG model are presented. The summary of the main parameters and the profiles of a well documented Tore Supra shot dedicated to electron heat transport studies are given in Sec. 3. Finally, the results of this 'tokamak case simulation' are listed and discussed in Sec. 4.

2. The ETG model

The model presented below is well described in [14]. Nevertheless, we recall some important points. First of all, because of the natural scale separation, we only

https://doi.org/10.1017/S0022377806004466 Published online by Cambridge University Press

simulate a thin plasma annulus, while keeping the periodicity in the poloidal and toroidal angles, θ and φ. The topology of the magnetic surfaces as follows: magnetic surfaces are circular, without Shafranov shift and are labelled by the radial coordinate $x = (r - r_{\rm s})/r_{\rm box}$, where $r_{\rm s}$ and $r_{\rm box}$ are the position in the plasma and the radial box size, respectively.

Starting from Braginskii's fluid equations for electrons [16], one can obtain three evolution equations for electron pressure, electric potential and parallel momentum. For simplification, we assume that the ion response is adiabatic, $\tilde{n}_{\rm i}/n_{\rm i0} = -e\tilde{\phi}/T_{\rm i}$. Finally, the quasi-neutrality equation $\tilde{n}_{\rm e}/n_0 = \tilde{n}_{\rm i}/n_0$ closes the system. The model, containing the main features of ETG turbulence, is as follows:

$$\partial_t \phi - A_n \partial_\theta \phi + 2\epsilon\omega_d(\phi - P) - \rho_*^2[\phi, \nabla_\perp^2 \phi] - \frac{\epsilon}{\rho_*}\nabla_\parallel(d_*^2\nabla_\perp^2\psi) + [\psi, d_*^2\nabla_\perp^2\psi]$$

$$= -D_\phi \nabla_\perp^4 \phi \tag{2.1}$$

$$\partial_t F - 2\epsilon\omega_d(d_*^2\nabla_\perp^2\psi) + [\phi, F] + \frac{\epsilon}{\rho_*}\nabla_\parallel(\phi - P) + [\psi, P] = D_F\nabla_\perp^2 F \tag{2.2}$$

$$\partial_t P + 2\Gamma(1-\tau)\omega_d\phi \; + 4\Gamma\epsilon\omega_d P + [\phi, P] + \Gamma\tau\frac{\epsilon}{\rho_*}\nabla_\parallel(d_*^2\nabla_\perp^2\psi) - \; \Gamma\tau[\psi, d_*^2\nabla_\perp^2\psi]$$

$$= D_P\nabla_\perp^2 P - \frac{\epsilon}{\rho_*}X_L|\nabla_\parallel|P \tag{2.3}$$

where ϕ is the electrostatic potential, ψ the fluctuating part of the vector potential, P the total electron pressure and F the quantity defined as $F \equiv \psi - d_\star^2\nabla_\perp^2\psi$; Ampere's law relates the vector potential and the parallel electron velocity by $v = d_\star^2\nabla_\perp^2\psi$. The ion temperature is assumed to be constant, so we define the temperature ratio τ as $\tau = T_{\rm e}/T_{\rm i}$. $\epsilon = r_{\rm s}/R$ is the inverse aspect ratio. Γ is a constant and is equal to $\frac{5}{3}$ in fluid theory.

Lengths are normalized to $r_{\rm s}$, the radial position of the annulus, and time is normalized to $r_{\rm s}^2 eB/cT_{\rm i}$. $A_n = r_{\rm s}/L_n$ and $A_T = r_{\rm s}/L_T$ are the normalized gradient scale lengths for density and temperature, respectively. Experimentally, the following relationship holds: $A_T^{\rm Exp.} = R/L_T = A_T/\epsilon$. Units of $n_{\rm e}T_{\rm i}$ for the electron pressure, $T_{\rm i}/e$ for the potential, $\tau^{-1/2}v_{\rm th,e} = (T_{\rm i}/T_{\rm e})^{1/2}(T_{\rm e}/m_{\rm e})^{1/2}$ for velocity, $e\tau^{-1/2}v_{\rm th,e}/T_{\rm i}$ for the vector potential and $cT_{\rm i}/eB$ for turbulent conductivity are employed.

The main control parameters are the normalized Larmor radius $\rho_\star = \rho_{\rm s,e}/r_{\rm s}$ with $\rho_{\rm s,e} \equiv (T_{\rm i}/m_{\rm e})^{1/2}/\omega_{\rm c,e}$, the normalized skin depth $d_\star = d_{\rm e}/r_{\rm s}$ with $d_{\rm e} \equiv c/\omega_{\rm pe}$ and the inverse aspect ratio $\epsilon = r_{\rm s}/R$. One can define a parameter $\beta = \rho_\star^2/d_\star^2$ which is related to the usual β through the relation $\beta_{\rm usual} = 2(1+\tau)\beta$. Furthermore, D_ϕ, D_F and D_P are small artificial coefficients set to damp the smallest spatial scales. The main damping mechanism is provided by parallel Landau damping, modelled by the $|\nabla_\parallel|$ term in (2.3), which stands for the operator whose representation in Fourier space is given by $|k_\parallel|$.

3. The #19542 Tore Supra shot

As explained in [2], the Tore Supra tokamak can be used effectively to study electron heat transport. Using fast wave electron heating (FWEH), one can achieve hot plasma with $T_{\rm e}(0) > 2T_{\rm i}(0)$, with little collisional coupling between the electron and the ion channels. In our case, we focus on a well-documented Tore Supra shot (#19542). For this shot, during the FWEH phase, a steady state is reached as

https://doi.org/10.1017/S0022377806004466 Published online by Cambridge University Press

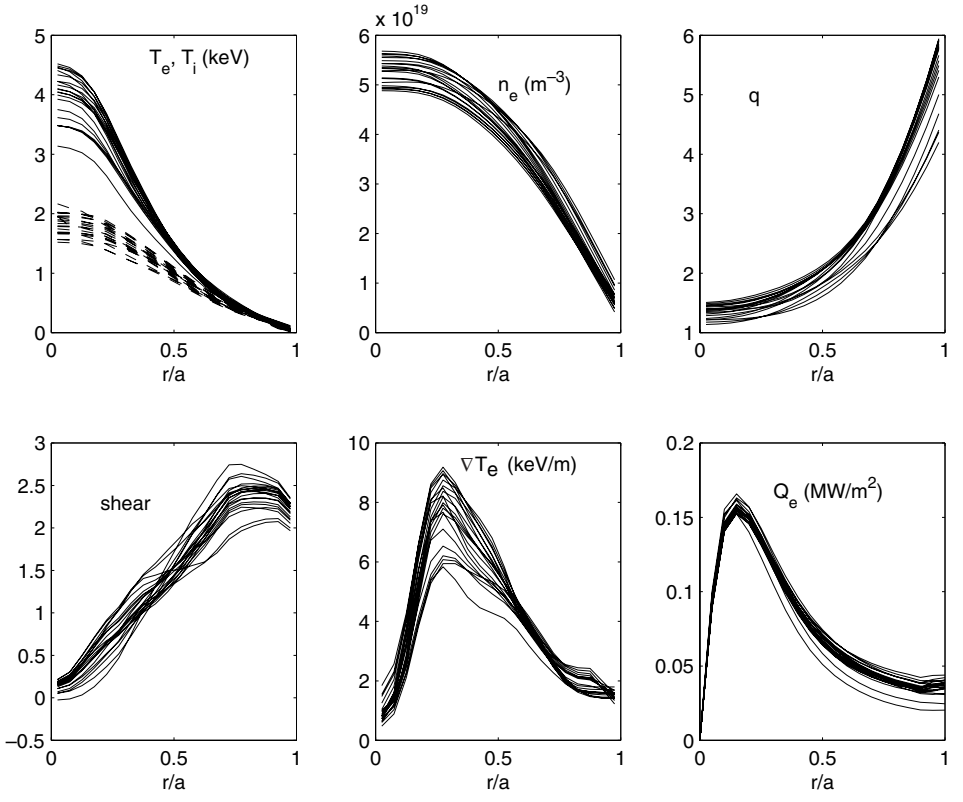


Figure 1. Temperature, density, safety factor, magnetic shear, electron temperature gradient and thermal flux profiles from $t = 5.3$ to 6.3 s in Tore Supra shot #19542.

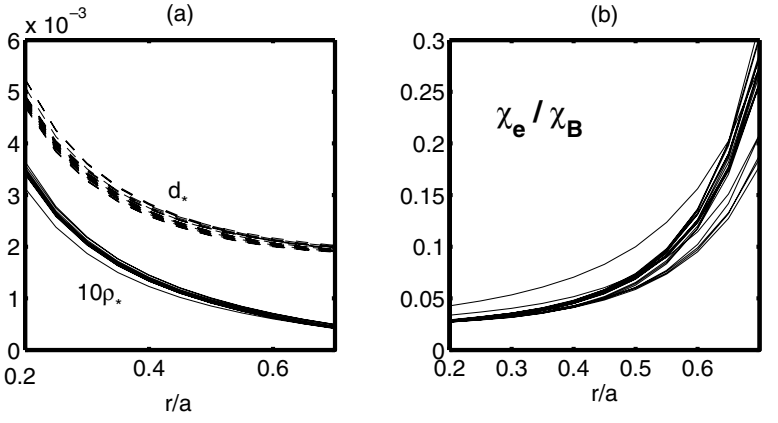


Figure 2. Normalized gyroradius and plasma skin depth (a) and normalized electron conductivity (b). The normalization length is $r_s = 0.38$ m and $\chi_B \equiv T_i/eB$.

the profiles reported in Fig. 1 show. We can see that the electron temperature in the plasma core exceeds the ion temperature by a factor of four. In Fig. 2, we have plotted the normalized electron gyroradius $\rho_\star = \rho_e/r_s$, the normalized skin

https://doi.org/10.1017/S0022377806004466 Published online by Cambridge University Press

depth $d_\star = d_\mathrm{e}/r_\mathrm{s}$ and the normalized electron conductivity $\chi_\mathrm{e}/\chi_\mathrm{B}$. The thermal electron conductivity χ_e is computed from the power balance and $\chi_\mathrm{B} \equiv T_\mathrm{i}/eB$. For the simulation, most parameters will be taken at $r/a = 0.5$. So, this gives as normalization length $r_\mathrm{s} = 0.5 \times \bar{a} \simeq 0.38$ m where $\bar{a}$ is the plasma minor radius averaged over shot duration while the major radius $R = 2.3$ m. The inverse aspect ratio, as defined in Sec. 2, is given by $\epsilon = r_\mathrm{s}/R \simeq 0.16$. We can evaluate the ratio $\beta \equiv \rho_\star^2/d_\star^2$ at this radial position and we find $\beta \simeq 0.16\%$. From this value, one can estimate τ through $\tau = \beta^{\mathrm{usual}}/2\beta - 1 \simeq 0.98$. This value is different from that estimated by $T_\mathrm{e}(r/a = 0.5)/T_\mathrm{i}(r/a = 0.5) \simeq 1.4$ mainly because it is difficult to estimate the ion temperature profile on Tore Supra. We have now to estimate the heat flux coming from the inner region ($r/a < 0.5$). This gives, in terms of 'code units', $\Gamma_\mathrm{inj}/\rho_\star \simeq 120$. Finally, we can estimate the critical temperature gradient value with the experimental formula given by Hoang et al. [17]: $R/L_{T,\mathrm{c}} = 5(\pm 1) + 10(\pm 2)|\hat{s}|/q$. At $r/a = 0.5$, we have $\hat{s} = 1$ and $q = 1.8$, so one finds

$$\left[\frac{R}{L_{T,\mathrm{c}}}\right]^{\#19542} = 10.5 \pm 2.1. \tag{3.1}$$

4. Simulation results and discussion

As explained above, for the so-called 'tokamak case simulation', we try to match, as closely as possible, the Tore Supra parameters at $r/a = 0.5$. The various parameters that we keep are as follows: the magnetic shear $\hat{s} = 1$, the safety factor $q = 1.8$ at the inner boundary, the ratio between temperatures $\tau = T_\mathrm{e}(x = 0.5)/T_\mathrm{i}(x = 0.5) = 1.4$, the inverse aspect ratio $\epsilon \simeq 0.16$ and $\beta^{\mathrm{Num}} = \rho_\star^2/d_\star^2 = 0.2\%$. The density gradient length is taken equal to zero, although, for the Tore Supra shot, this value is equal to one, roughly. Nevertheless, it is known that a steep density profile stabilizes the ITG/ETG modes. The normalized temperature gradient length at the inner boundary is fixed at the value -2 while the collisional conductivity at $x = 0$ will take three values. The resulting injected flux is then $\Gamma_\mathrm{inj} = -\chi_\mathrm{coll} \times \nabla_x T|_{x=0} = \{0.3; 1; 2\}$. For numerical reasons, the normalized electron Larmor radius $\rho_\star^{\mathrm{Num}}$, which is a fundamental parameter, is much lower than $\rho_\star^{\mathrm{Exp}}$. This parameter is equal to 0.02 in the simulation and that gives $\rho_\star^{\mathrm{Num}}/\rho_\star^{\mathrm{Exp}} \simeq 200$. In spite of this restriction, one sees that the maximum normalized injected fluxes are of the same order of magnitude:

$$\frac{[\Gamma_\mathrm{inj}/\rho_\star]^{\mathrm{Exp}}}{[\Gamma_\mathrm{inj}/\rho_\star]^{\mathrm{Num}}} \simeq 1.2. \tag{4.1}$$

The spatial resolution is $161 \times 128 \times 32$ for the radial, poloidal and toroidal directions, respectively. Because of the very high level of injected flux and the resulting steep gradients, the numerical time step is reduced by a factor of eight compared with previous simulations with the same $\rho_\star$. Notwithstanding this limitation, we evolve the system until it reaches a turbulent steady state for the three injected flux values we are testing. As in our previous studies [14], we look at the fluctuations in a poloidal cross section. Figure 3 shows the poloidal fluctuations for the pressure, the electric potential and the magnetic potential for the present simulation. The picture was taken at the end of the simulation when the injected flux is the maximum. Clearly, the turbulent cells are almost isotropic and not particularly elongated in the radial direction. This isotropization is due to the small value of the inverse

https://doi.org/10.1017/S0022377806004466 Published online by Cambridge University Press

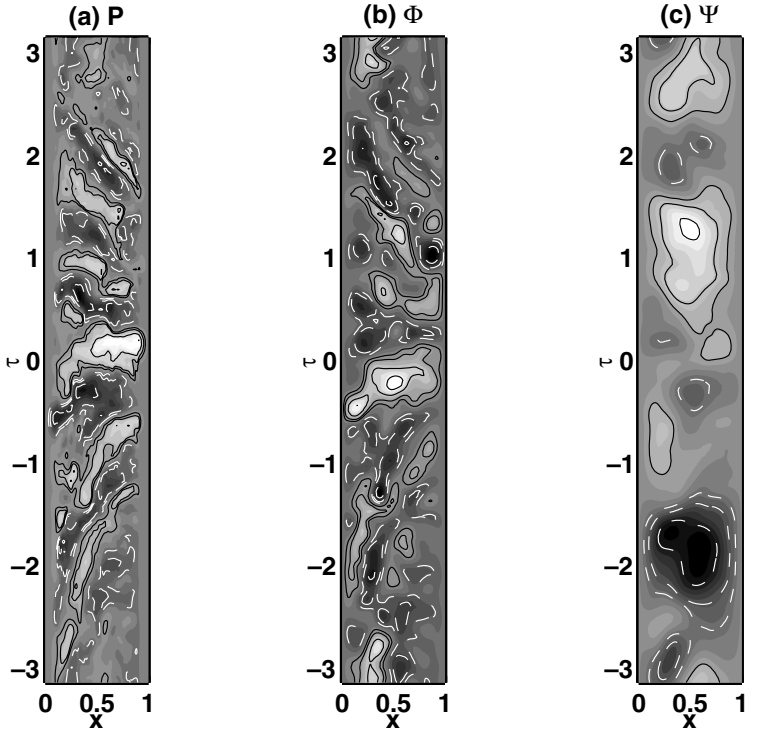


Figure 3. Fluctuations in a poloidal cross section for the pressure (a), the electric potential (b) and the magnetic potential (c). $\rho_\star = 0.02$ and $\Gamma_{\rm inj} = 2$ in this case.

aspect ratio. Such a value reduces the linear threshold and so the injected flux can bring the system very far from marginality and so destroy the typical radially elongated linear structures. Moreover, when $\epsilon \to 0$, as in the present case, one moves from toroidal to slab geometry, and so the curvature strength is weaker [13] and modes are less ballooned.

As far as the heat transport is concerned, the most important results are summarized in Fig. 4. We have plotted the averaged normalized turbulent conductivity $\chi_{\rm T}/\chi_{\rm gB}$, with the so-called gyro-Bohm conductivity $\chi_{\rm gB} \equiv \chi_{\rm B}/\rho_\star$, versus the normalized temperature gradient length L_T/R for the three values of injected flux. The average is made over the turbulent region $0.2 \leqslant x \leqslant 0.8$. The various points represent the temporal evolution of both quantities, the gradient and the conductivity. When the turbulent steady state is reached, an accumulation of points is formed, giving an averaged conductivity and an averaged gradient for a given injected heat flux. The critical temperature gradient for this nonlinear simulation is estimated by fitting the points corresponding to a turbulent steady state with a straight line (see Fig. 4). This line cuts the abscissa axis at the critical temperature gradient, the gradient below which there is no any turbulent transport. By this method, we find a critical temperature gradient equal to

$$\left[\frac{R}{L_{T,\rm c}}\right]^{\rm Num} \simeq 12. \tag{4.2}$$

https://doi.org/10.1017/S0022377806004466 Published online by Cambridge University Press

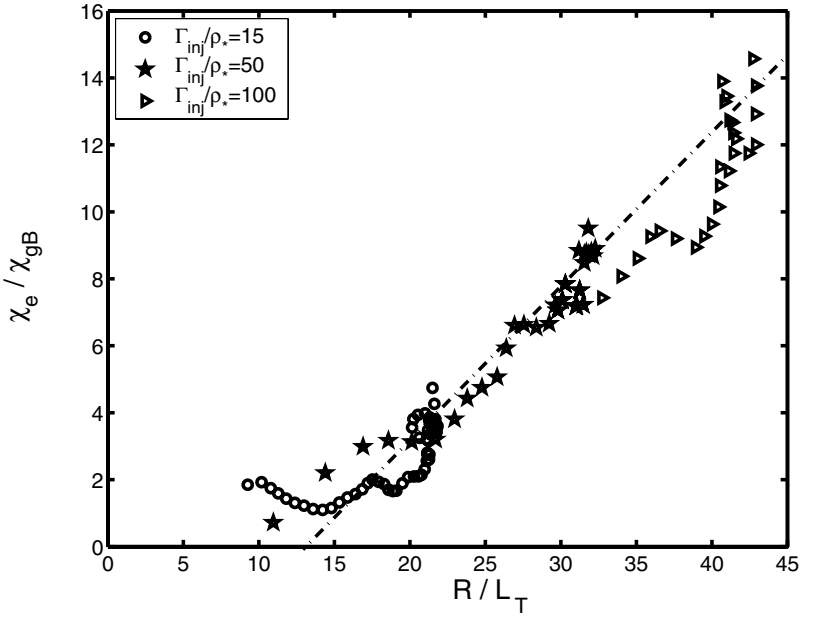


Figure 4. Normalized turbulent conductivity versus the normalized temperature gradient for the simulation. The line fits the points where the turbulent steady state is reached (see the text).

This value is not very far from the experimental value estimated for this shot (3.1). Usually, it seems that fluid models underestimate the critical temperature gradients compared with the experimental estimations and the gyrokinetic simulations. Now, we focus on the comparison between the simulated turbulent conductivity and the experimental one estimated from the power balance. If one assumes that the heat transport is gyro-Bohm, we must normalize the conductivities to $\chi_{\mathrm{gB}} \equiv \chi_{\mathrm{B}}/\rho_\star$ to make a meaningful comparison. Doing so, we can calculate the ratio of the experimental conductivity (Fig. 2) to the simulated conductivity taken at the maximum injected heat flux (Fig. 4). One finds

$$\frac{[\chi_{\mathrm{e}}/\chi_{\mathrm{gB}}]^{\mathrm{Exp}}}{[\chi_{\mathrm{e}}/\chi_{\mathrm{gB}}]^{\mathrm{Num}}} \simeq \frac{600}{14} \simeq 45. \tag{4.3}$$

This ratio obviously shows that our simulation cannot reproduce the experimental conductivity. For a given injected flux, one sees that the simulation will increase substantially the normalized gradient and not increase the conductivity much. Conversely, the electron heat losses experience, for a similar level of injected flux, a large conductivity associated with a normalized gradient very close to the critical value $L_T \simeq L_{T,\mathrm{e}}$. This phenomenon, reported as *stiffness*, has been observed in many tokamaks [18]. One possible explanation for this absence of stiffness could be the limitation in the $\rho_\star$ excursion. Lower values for this parameter cannot be reached without some improvements in the present numerical code. The gyro-Bohm scaling for the heat conductivity has been observed in both numerical simulations [14] and experiments [19], but recent girokinetic simulations [11] show a Bohm-like scaling for the ETG-related heat transport. In [11], the authors claim that this

https://doi.org/10.1017/S0022377806004466 Published online by Cambridge University Press

scaling could explain the difference between flux-tube and global simulations. We have also to note that in the gyrokinetic flux-tube simulations, in which the ETG turbulent transport is found to be sufficiently large, the parameter L_T is fixed, while in our approach the heat flux is frozen and the gradient is free to evolve, which is a closer approach to what occurs in a tokamak.

This difference, which can be summarized as local *versus* global simulations, might be a factor in the observed discrepancy. This is partly confirmed by recent global gyrokinetic simulations [12]. In any case, this subject is well beyond the aim of the present paper and a more refined cross-check between this type of fluid simulation and global gyrokinetic simulations is needed. Finally, the large observed difference between numerical and experimental heat conductivities imposes the conclusion that the anomalous electron heat transport cannot be explained by a global fluid model based on the ETG-driven instability.

Acknowledgements

BL would like to mention that these simulations have been performed on computing resources of the Département de Recherches sur la Fusion Contrôlée—CEA Cadarache. The authors would also like to thank Y. Idomura, X. Garbet and G. T. Hoang for their support and for fruitful discussions.

References

[1] Horton, W., Choi, D.-I. and Tang, W. M. 1981 *Phys. Fluids* **24**, 1077–1085.
[2] Horton, W. et al. 2000 *Phys. Plasmas* **7**, 1494.
[3] Ohkawa, T. 1978 *Phys. Lett.* A **67**, 35.
[4] ITER Physics Basis 1999 *Nucl. Fusion* **39**, 12.
[5] Horton, W., Hong, B. G. and Tang, W. M. 1988 *Phys. Fluids* **31**, 2971.
[6] Kim, J. Y. and Horton, W. 1991 *Phys. Fluids* B **3**, 3194–3197.
[7] Horton, W., Hong, B.-G., Tajima, T. and Bekki, N. 1990 *Comm. Plasma Phys. Control. Fusion* **13**, 207–217.
[8] Jenko, F. et al. 2000 *Phys. Plasmas* **7**, 5, 1904.
[9] Dorland, W., Jenko, F., Kotschenreuther, M. and Rogers, B. N. 2000 *Phys. Rev. Lett.* **85**, 5579.
[10] Jenko, F. and Dorland, W. 2001 *Plasmas Phys. Control. Fusion* **43**, A-141.
[11] Idomura, Y., Tokuda, S. and Kishimoto, Y. 2005 *Nucl. Fusion* **45**, 1571.
[12] Lin, Z., Chen, L. and Zonca, F. 2005 *Phys. Plasmas* **12**, 056125.
[13] Labit, B. 2003 Electron heat transport in tokamaks by direct numerical simulation of small scale turbulence. PhD thesis, Université de Provence (in French).
[14] Labit, B. and Ottaviani, M. 2003 *Phys. Plasmas* **10**, 126.
[15] Aymar, R. 1989 *Plasma Physics and Controlled Nuclear Fusion Research (Proc. 12th Int. Conf., Nice, 1988, Vol. 1.)* Vienna: IAEA, p. 9.
[16] Braginskii, S. I. 1965 *Reviews of Plasmas Physics*, Vol. I, (ed. M. A. Leontovitch). New York: Consultants Bureau, p. 205.
[17] Hoang, G. T., Bourdelle, C., Garbet, X., Giruzzi, G., Aniel, T., Ottaviani, M., Horton, W., Zhu, P. and Budny, R. V. 2001 *Phys. Rev. Lett.* **87**, 12.
[18] Ryter, F. et al. 2001 *Plasma Phys. Control. Fusion* **43**, A323–A338.
[19] Zou, X. L. et al. 1999 Investigation of dimensionless scaling laws and non local transport in Tore Supra. In: *Proc. 17th IAEA Fusion Energy Conf., Yokohama, Japan*. Vienna: IAEA, EXP/P2-13.

https://doi.org/10.1017/S0022377806004466 Published online by Cambridge University Press